Cell Host & Microbe, Volume *29*

Supplemental information

Potent SARS-CoV-2 neutralizing antibodies directed against spike N-terminal domain target a single supersite

Gabriele Cerutti, Yicheng Guo, Tongqing Zhou, Jason Gorman, Myungjin Lee, Micah Rapp, Eswar R. Reddem, Jian Yu, Fabiana Bahna, Jude Bimela, Yaoxing Huang, Phinikoula S. Katsamba, Lihong Liu, Manoj S. Nair, Reda Rawi, Adam S. Olia, Pengfei Wang, Baoshan Zhang, Gwo-Yu Chuang, David D. Ho, Zizhang Sheng, Peter D. Kwong, and Lawrence Shapiro

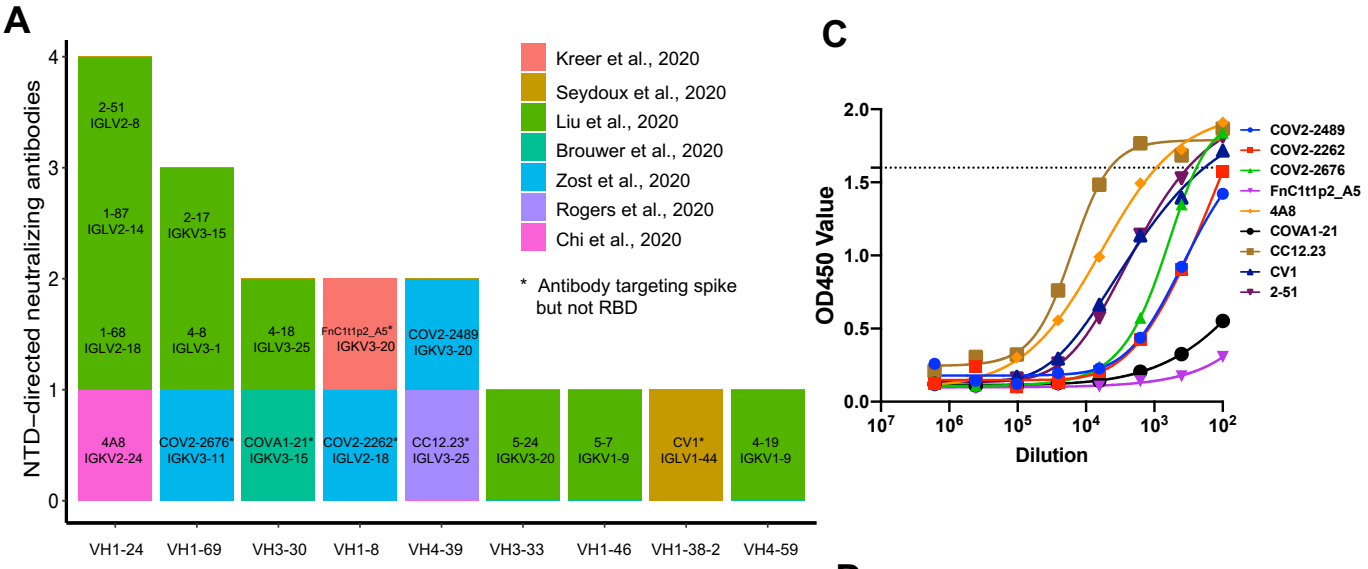

B

mAb	HV	LV	Neutralization IC50 (μg/mL)	Neutralization strain	Live virus (USA/WA1) neutralization IC50 (μg/mL)	Epitope	Reference
COV2-2489	HV4-39	KV3-20	16.	USA-WA1/2020*	0.009	NTD	Zost et al., 2020
COV2-2262	HV1-8	LV2-18	6.0	USA-WA1/2020*	0.014	NTD	Zost et al., 2020
COV2-2676	HV1-69	KV3-11	9.6	USA-WA1/2020*	0.004	NTD	Zost et al., 2020
FnC1t1p2_A5	HV1-8	KV3-20	16.	BavPat1/2020#	0.062	S, Non-RBD	Kreer et al., 2020
4A8	HV1-24	KV2-24	0.61	Not mentioned^	<0.0032	NTD	Chi et al., 2020
COVA1-21	HV3-30	KV3-15	0.16	BY-ChVir-929/2020$	0.083	NTD	Brouwer et al., 2020
CC12.23	HV4-39	LV3-25	8.7	USA-WA1/2020&	9.365	S, Non-RBD	Rogers et al., 2020
CV1	HV4-38-2	LV1-44	15.	Pseudo virus	3.207	NTD	Seydoux et al., 2020
4-8	HV1-69	LV3-1	0.009	USA-WA1/2020@	0.016	NTD	Liu et al., 2020
1-68	HV1-24	LV2-18	0.014	USA-WA1/2020@	0.003	NTD	Liu et al., 2020
1-87	HV1-24	LV2-14	0.086	USA-WA1/2020@	0.009	NTD	Liu et al., 2020
2-51	HV1-24	LV2-8	0.007	USA-WA1/2020@	0.01	NTD	Liu et al., 2020
5-24	HV3-33	KV3-20	0.008	USA-WA1/2020@	0.003	NTD	Liu et al., 2020
4-19	HV4-59	KV1-9	0.109	USA-WA1/2020@	0.109	NTD	Liu et al., 2020
4-18	HV3-30	LV3-25	0.020	USA-WA1/2020@	0.054	NTD	Liu et al., 2020
5-7	HV1-46	KV1-9	0.033	USA-WA1/2020@	0.033	NTD	Liu et al., 2020
2-17	HV1-69	KV3-15	0.007	USA-WA1/2020@	0.036	NTD	Liu et al., 2020

*: An automated real-time cell analysis (RTCA) rapid screening assay19 that allows quantitation of cytopathic effect (CPE) with WA1/2020 strain SARS-CoV-2 in Vero-furin cells.
#: Absence of CPE (BavPat1/2020 strain) compared to virus controls on VeroE6 cells (ATCC CRL-1586).
^: Sera or antibodies were serially diluted and then mixed with 100 TCID50 SARS-CoV-2. The mixture was moved to the wells containing Vero-E6 cells and incubated at 37 ℃ for 1h.
$: Neutralization capacity against SARS-CoV-2 (German isolate, BY-ChVir-929/2020 strain) on Vero-E6 cells.
&: Neutralization assay against USA-WA1/2020 strain on HeLa-ACE2 cells.
@: Neutralization assay against authentic SARS-CoV-2 (strain USA-WA1/2020) on Vero-E6 cells

D

AUC		Competitor antibody						
		COV2-2489	COV2-2262	COV2-2676	4A8	2-51	CC12.23	CV1
Biotinylated antibody	COV2-2489	586	764	654	613	599	813	964
	COV2-2262	594	497	514	308	343	982	772
	COV2-2676	692	888	547	618	775	993	1018
	4A8	509	490	481	188	152	700	1075
	2-51	573	508	419	169	158	877	1073
	CC12.23	1086	1056	917	957	972	184	983
	CV1	1049	1049	1053	1060	1215	1017	352

E

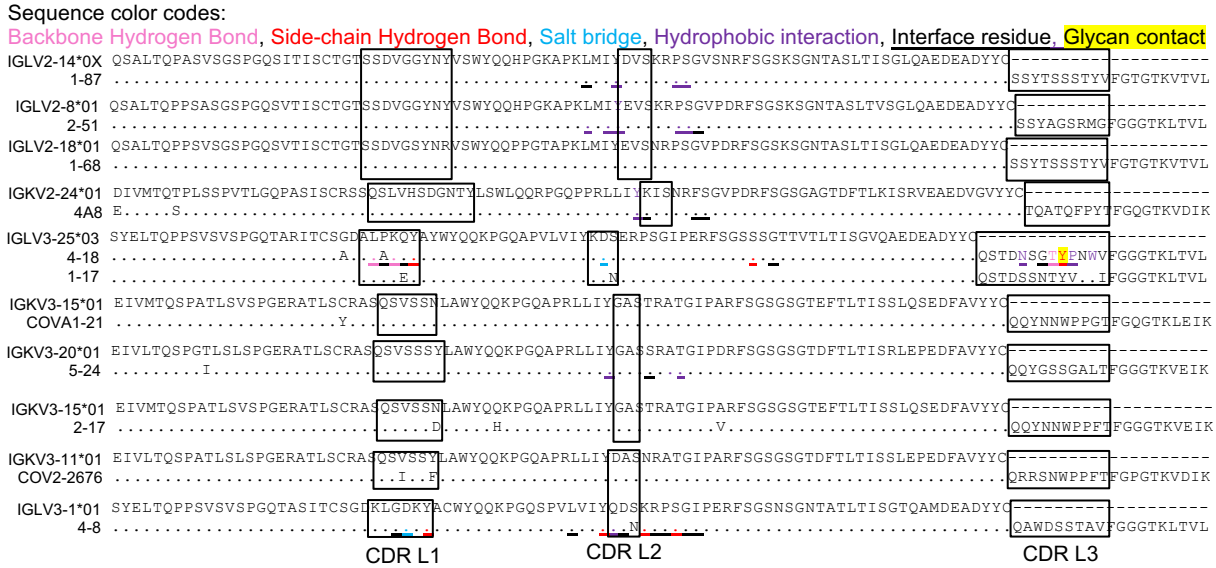

Figure S1. NTD-directed neutralizing antibodies isolated from convalescent donors show enrichment of four VH genes, Related to Figures 1-3.

(A) Published SARS-CoV-2 neutralizing antibodies targeting NTD or non-RBD spike epitopes (two additional NTD-directed neutralizing class members were reported recently FC05 and CM25 (Voss et al., 2020; Wang et al., 2021); both are derived from the VH1-24 heavy chain and are not included in this analysis).
(B) Table of published NTD antibodies with neutralization data. Live virus (USA/WA1) neutralization data was measured by the same batch of USA/WA1 strain.
(C) Binding curve of NTD antibodies with spike S2P.
(D) ELISA competition assay for NTD antibodies.
(E) Light chain sequence alignment for VH1-24-derived antibodies, for VH3-30/33-derived antibodies, and for VH1-69-derived antibodies. 1-87 was assigned to a novel germline gene IGLV1-24*0X.

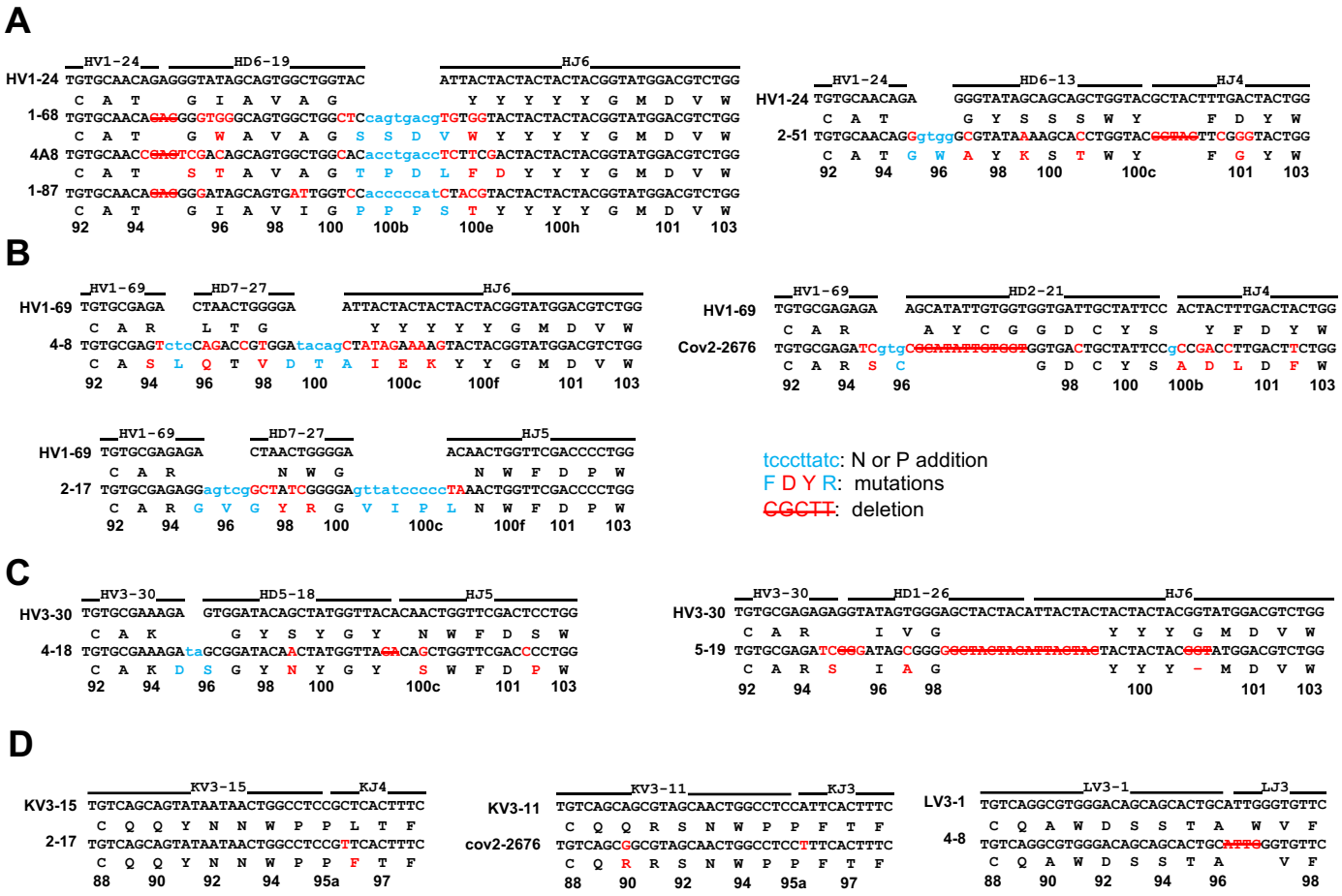

Figure S2. CDR H3 VDJ junction analysis for NTD neutralizing antibodies and CDR L3 VJ junction analysis for antibodies derived from VH1-69, Related to Figures 1-3.

Germline nucleotide and amino acid residues are shown in black with the corresponding junctions colored in light blue. Somatic hypermutations are colored in red. Nucleotides deleted by exonuclease trimming are indicated with strikethrough. The lower-case blue nucleotides represent the N and P nucleotide additions at the junctions.

(A) VH1-24-derived antibodies.
(B) VH1-69-derived antibodies.
(C) VH3-30/33-derived antibodies.
(D) Light chain VH junctional analysis for VH1-69-derived antibodies.

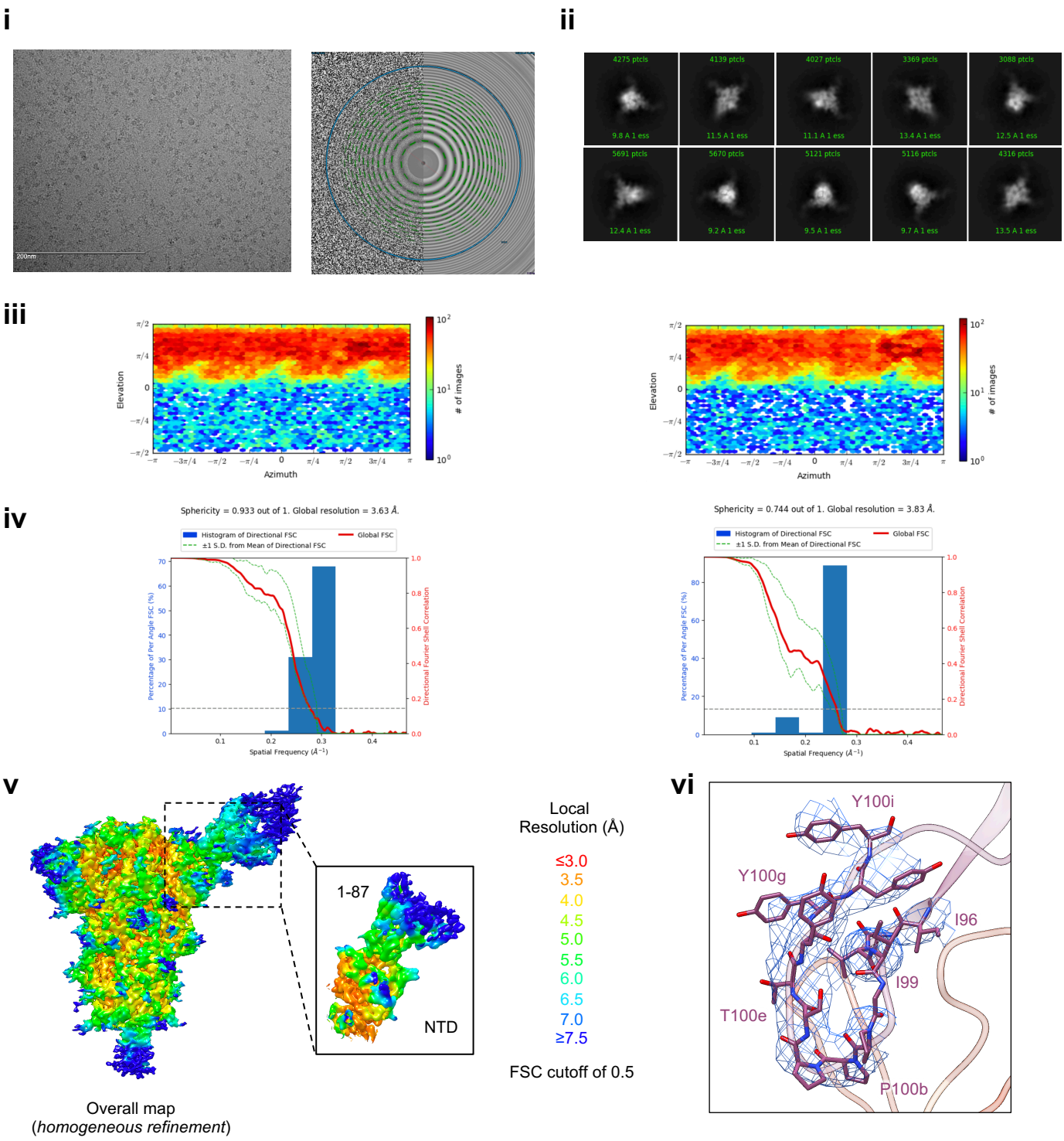

Figure S3A. Cryo-EM details of 1-87 Fab in complex with SARS-CoV-2 S2P spike, Related to Figure 1.

(i) Representative micrograph and CTF of the micrograph are shown. Micrograph scale bars (200 nm, white) are shown in the lower left of the images.

(ii) Representative 2D class averages are shown.

(iii) Angular distribution plots showing the orientations of all particles used in the final refinement as a heatmap for the overall map (left panel) and the locally refined map (right panel).

(iv) 3D FSC analysis was used to calculate the gold-standard Fourier shell correlation and the resolution anisotropy of the final maps. The FSC resulted in a resolution of 3.63 Å for the overall map (left panel) and 3.83 Å for the masked local refinement of the NTD:1-87 interface (right panel). Resolution anisotropy was assessed by calculating sphericity values, that resulted in 0.933 for the overall map and 0.744 for the locally refined map; the observed anisotropy did not preclude the generation of a high-quality map for an accurate modeling of the NTD:1-87 interface.

(v) The local resolution of the final overall map and locally refined map are shown, generated through cryoSPARC using an FSC cutoff of 0.5.

(vi) Representative density is shown for the CDR H3 loop of 1-87 contacting NTD; the contour level is 2.1σ. CDR H3 carbon atoms are colored in magenta, oxygen in red, nitrogen in blue; NTD is colored in orange.

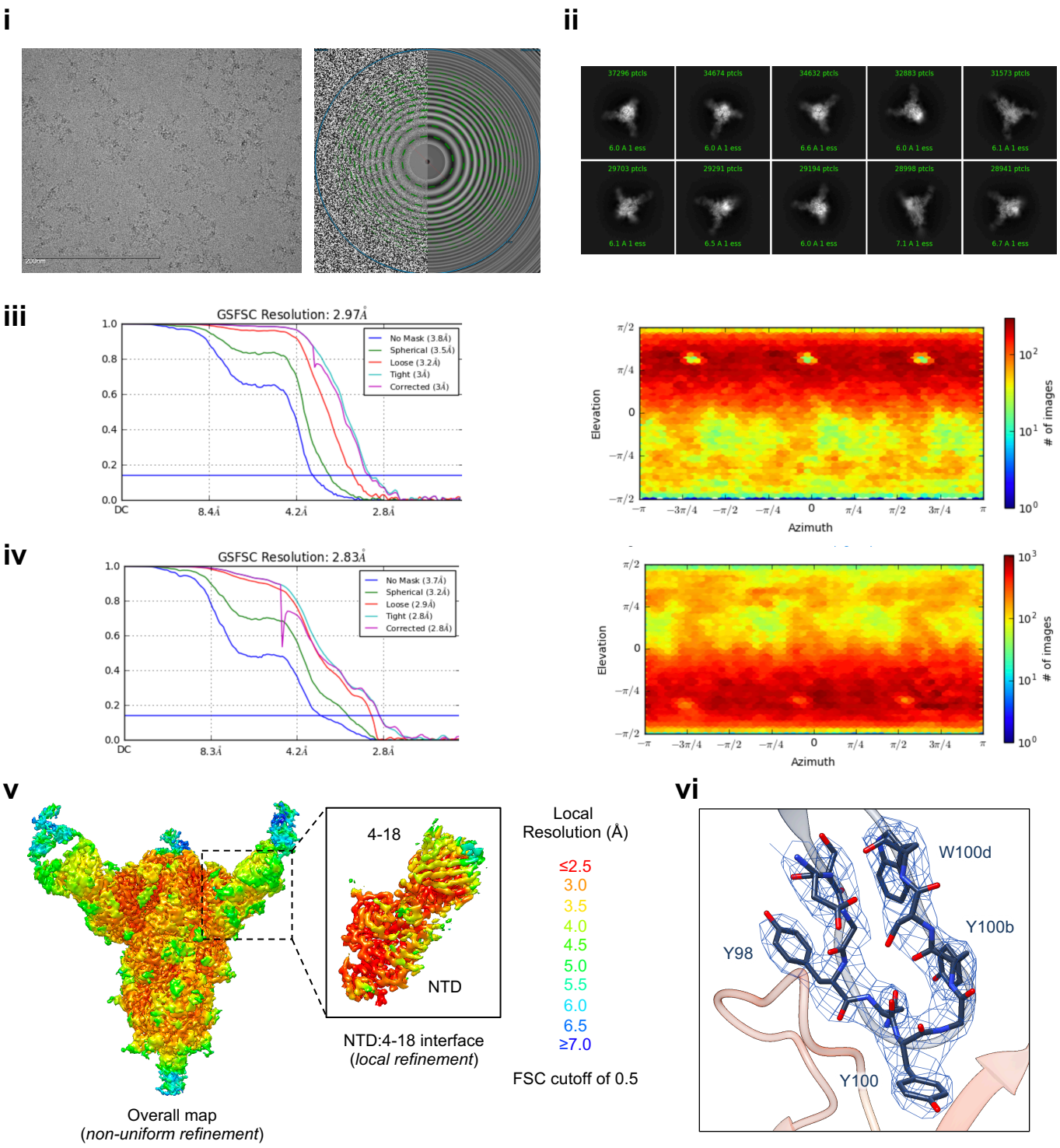

Figure S3B. Cryo-EM details of 4-18 Fab in complex with SARS-CoV-2 S2P spike, Related to Figure 2.

(i) Representative micrograph and CTF of the micrograph are shown. Micrograph scale bars (200 nm, white) are shown in the lower left of the images.

(ii) Representative 2D class averages are shown.

(iii) The gold-standard Fourier shell correlation resulted in a resolution of 2.97 Å for the overall map using non-uniform refinement (left panel); the orientations of all particles used in the final refinement are shown as a heatmap (right panel).

(iv) The gold-standard Fourier shell correlation resulted in a resolution of 2.83 Å for the masked local refinement of the NTD:4-18 interface (left panel) obtained using symmetry expansion in C3; the orientations of all particles used in the local refinement are shown as a heatmap (right panel).

(v) The local resolution of the final overall map and locally refined map are shown, generated through cryoSPARC using an FSC cutoff of 0.5.

(vi) Representative density is shown for the CDR H3 loop of 4-18 contacting NTD; the contour level is 1.4σ. CDR H3 carbon atoms are colored in dark blue, oxygen in red, nitrogen in blue; NTD is colored in orange.

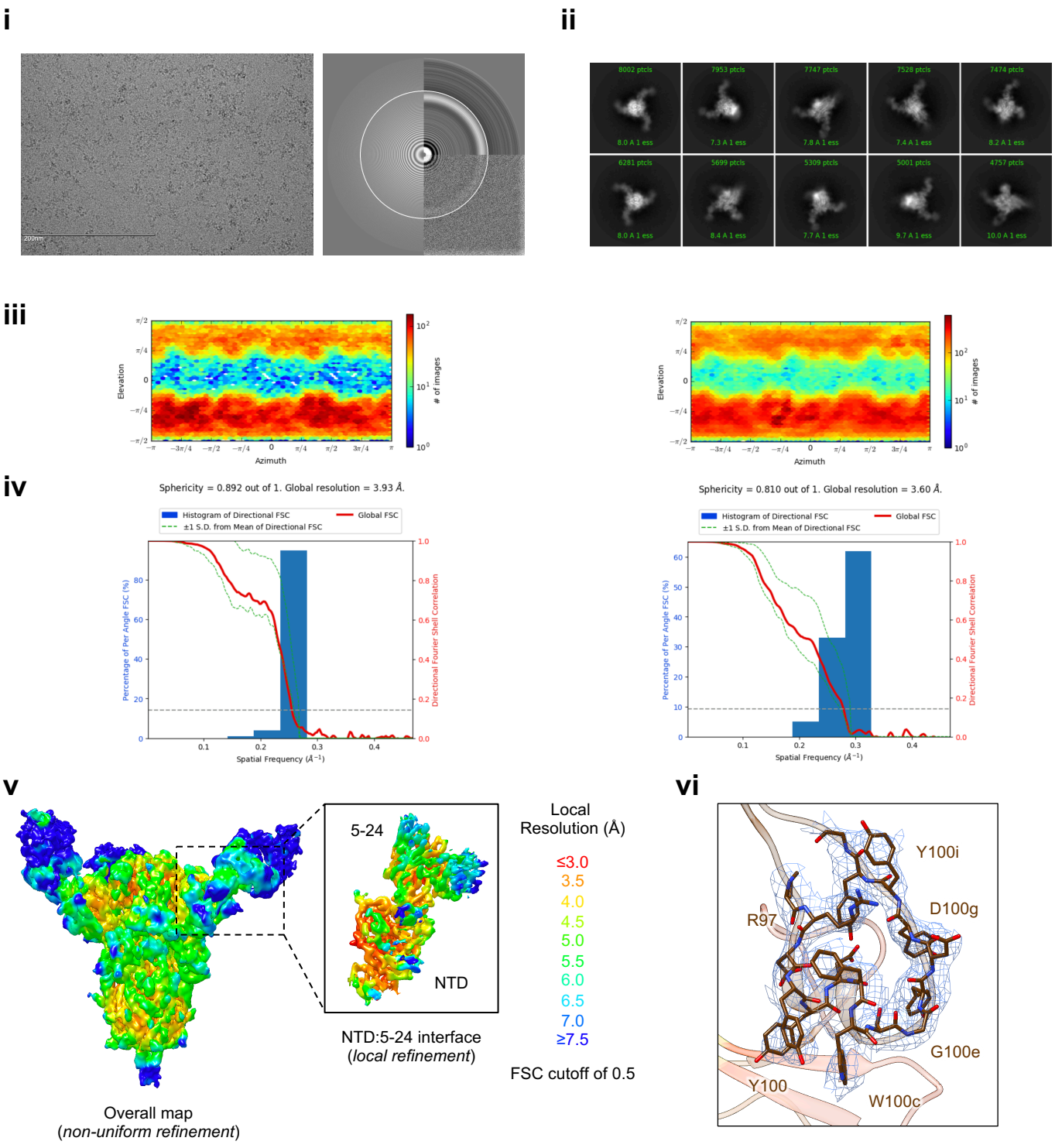

Figure S3C. Cryo-EM details of 5-24 Fab in complex with SARS-CoV-2 S2P spike, Related to Figure 2.

(i) Representative micrograph and CTF of the micrograph are shown. Micrograph scale bars (200 nm, white) are shown in the lower left of the images.

(ii) Representative 2D class averages are shown.

(iii) Angular distribution plots showing the orientations of all particles used in the final refinement as a heatmap for the overall map (left panel) and the locally refined map (right panel).

(iv) 3D FSC analysis was used to calculate the gold-standard Fourier shell correlation and the resolution anisotropy of the final maps. The FSC resulted in a resolution of 3.93 Å for the overall map (left panel) and 3.60 Å for the masked local refinement of the NTD:5-24 interface (right panel) obtained using symmetry expansion in C3. Resolution anisotropy was assessed by calculating sphericity values, that resulted in 0.892 for the overall map and 0.810 for the locally refined map; the observed anisotropy did not preclude the generation of a high-quality map for an accurate modeling of the NTD:5-24 interface.

(v) The local resolution of the final overall map and locally refined map are shown, generated through cryoSPARC using an FSC cutoff of 0.5.

(vi) Representative density is shown for the CDR H3 loop of 5-24 contacting NTD; the contour level is 1.7σ. CDR H3 carbon atoms are colored in brown, oxygen in red, nitrogen in blue; NTD is colored in orange.

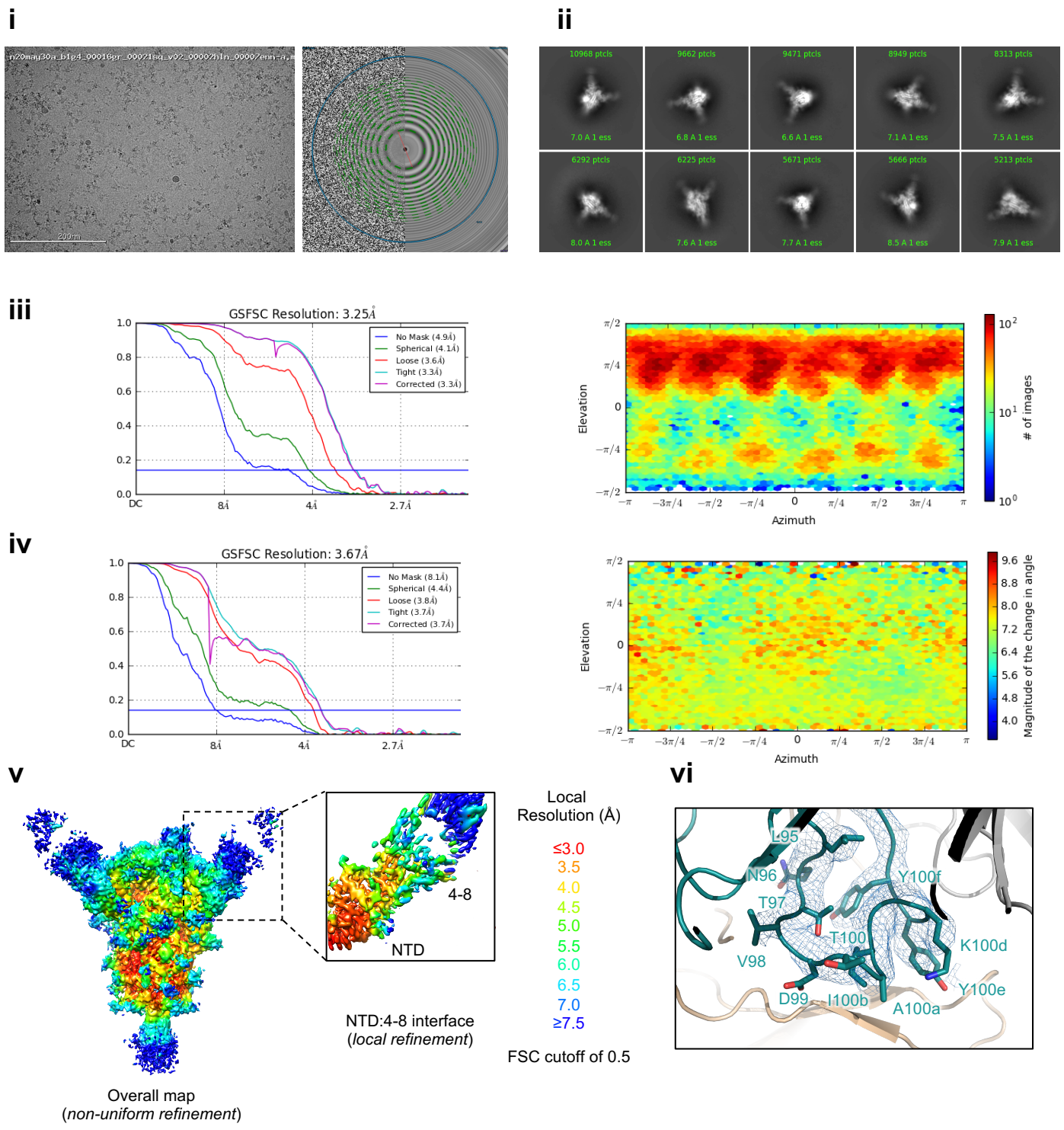

Figure S3D. Cryo-EM details of 4-8 Fab in complex with SARS-CoV-2 S2P spike, Related to Figure 3.

(i) Representative micrograph and CTF of the micrograph are shown. Micrograph scale bars (200 nm, white) are shown in the lower left of the images.

(ii) Representative 2D class averages are shown.

(iii) The gold-standard Fourier shell correlation resulted in a resolution of 3.25 Å for the overall map using non-uniform refinement with C1 symmetry (left panel); the orientations of all particles used in the final refinement are shown as a heatmap (right panel).

(iv) The gold-standard Fourier shell correlation resulted in a resolution of 3.67 Å for the masked local refinement of the NTD:4-8 interface (left panel) obtained using particle subtraction followed by local refinement; the orientations of all particles used in the local refinement are shown as a heatmap (right panel).

(v) The local resolution of the final overall map and locally refined map are shown, generated through cryoSPARC using an FSC cutoff of 0.5.

(vi) Representative density is shown for the CDR H3 loop of 4-8 contacting NTD; the contour level is 1.5σ. CDR H3 carbon atoms are colored in dark teal, oxygen in red, nitrogen in blue; NTD is colored in orange.

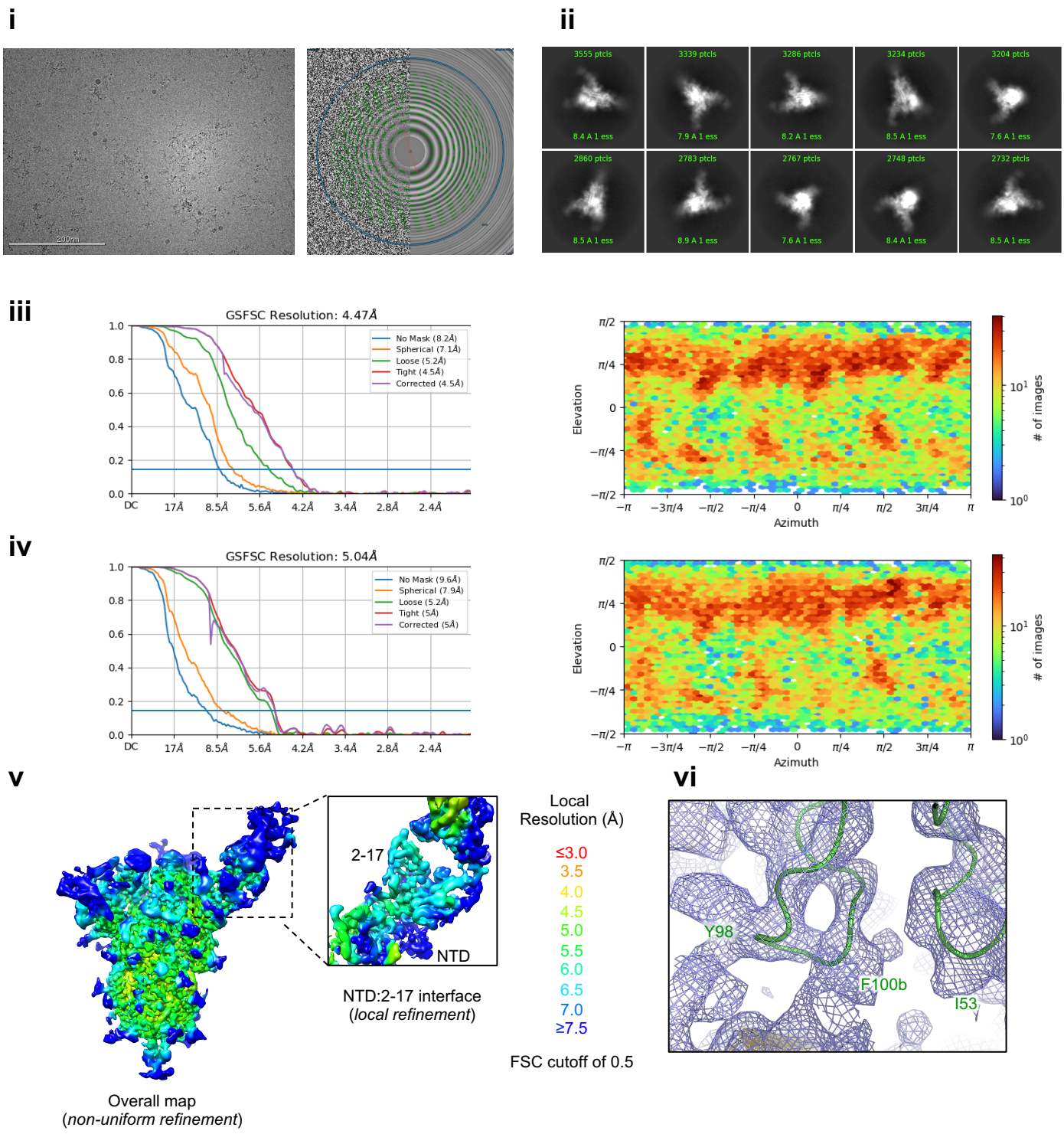

Figure S3E. Cryo-EM details of 2-17 Fab in complex with SARS-CoV-2 S2P spike, Related to Figure 3.

(i) Representative micrograph and CTF of the micrograph are shown. Micrograph scale bars (200 nm, white) are shown in the lower left of the images.

(ii) Representative 2D class averages are shown.

(iii) The gold-standard Fourier shell correlation resulted in a resolution of 4.47 Å for the overall map using non-uniform refinement with C1 symmetry (left panel); the orientations of all particles used in the final refinement are shown as a heatmap (right panel).

(iv) The gold-standard Fourier shell correlation resulted in a resolution of 5.04 Å for the masked local refinement of the NTD:2-17 interface (left panel); the orientations of all particles used in the local refinement are shown as a heatmap (right panel).

(v) The local resolution of the final overall map and locally refined map are shown, generated through cryoSPARC using an FSC cutoff of 0.5.

(vi) Representative density is shown for the CDR H3 loop of 2-17 contacting NTD; the contour level is 1.5σ. CDR H3 carbon atoms are colored in dark green; NTD is colored in orange. Due to limited resolution only the main chain was modeled, although density for some larger side chains such as Y98 and F100b are shown.

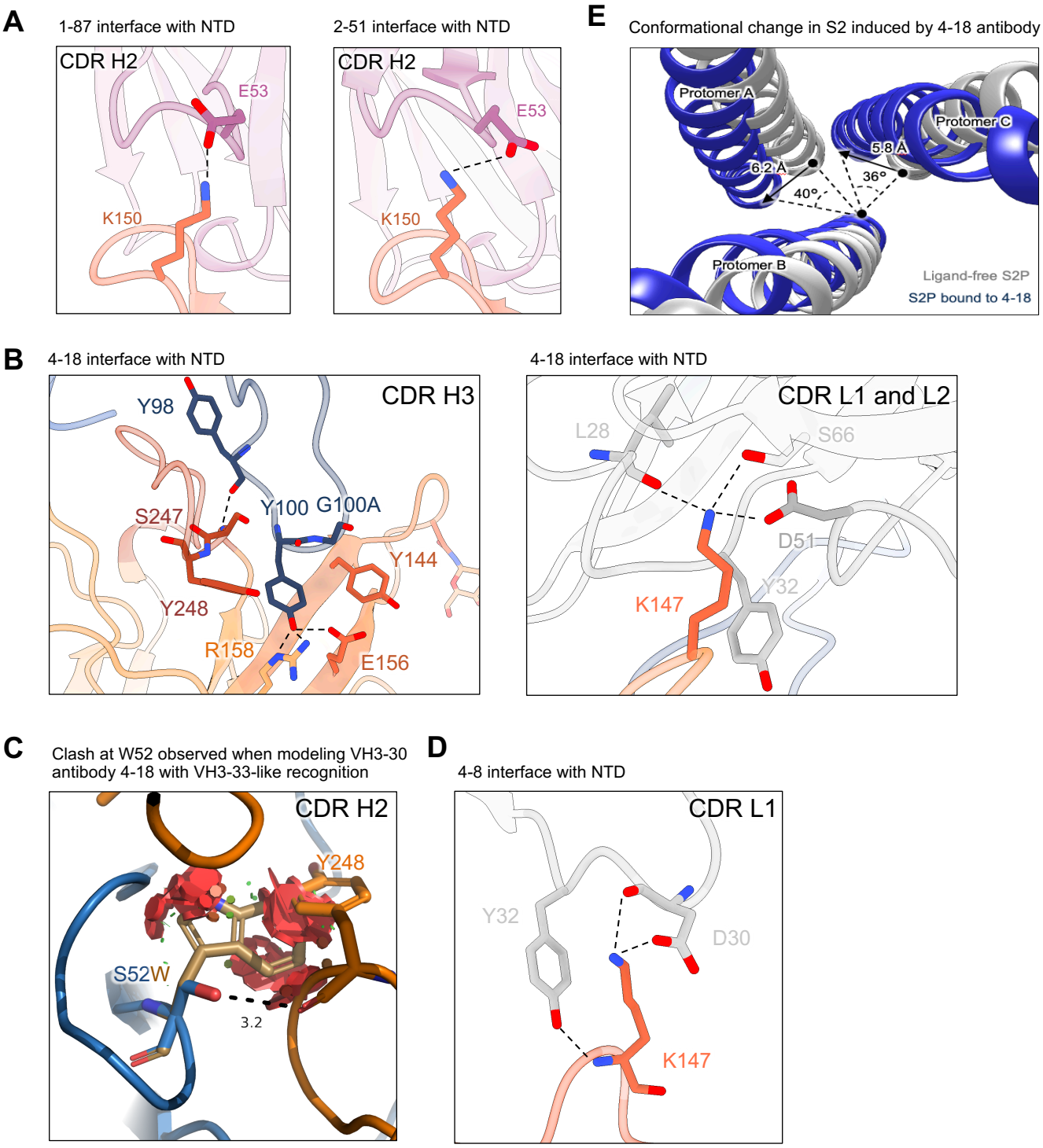

Figure S4. Additional observations from 1-87, 4-18 and 4-8 complexes, Related to Figures 1-3.

(A) The main interaction observed in CDR H2 for VH1-24-derived antibodies is a salt bridge between Glu53 and Lys150, observed in both 1-87 (left panel) and 2-51 (right panel). NTD is colored in orange; CDHR H2 is colored in magenta. Nitrogen atoms are colored in blue, oxygen atoms in red; hydrogen bonds are represented as dashed lines.

(B) Expanded view of 4-18 interactions with NTD showing recognition in CDR H3 (left panel), and recognition in CDR L1 and L2 (right panel). NTD regions N3 (residues 141-156) and N5 (residues 246-260) are colored in shades of orange; CDR H3 is colored in dark blue; CDR L1 and L2 are colored in shades of gray.

(C) The S52W substitution between VH3-30 and VH3-33 is incompatible with the binding mode of 4-18. Mutating Ser52 (blue) to Tryptophane (brown) would bring major steric clashes (red plate) between 4-18 heavy chain (blue) and NTD (orange). The hydrogen bond between Ser52 and Tyr248 on NTD is represented as a dashed line.

(D) Expanded view of 4-8 interactions with NTD showing recognition in CDR L1, colored as in (B)

(E) Conformational change in the S2 region of spike induced by 4-18 antibody binding.

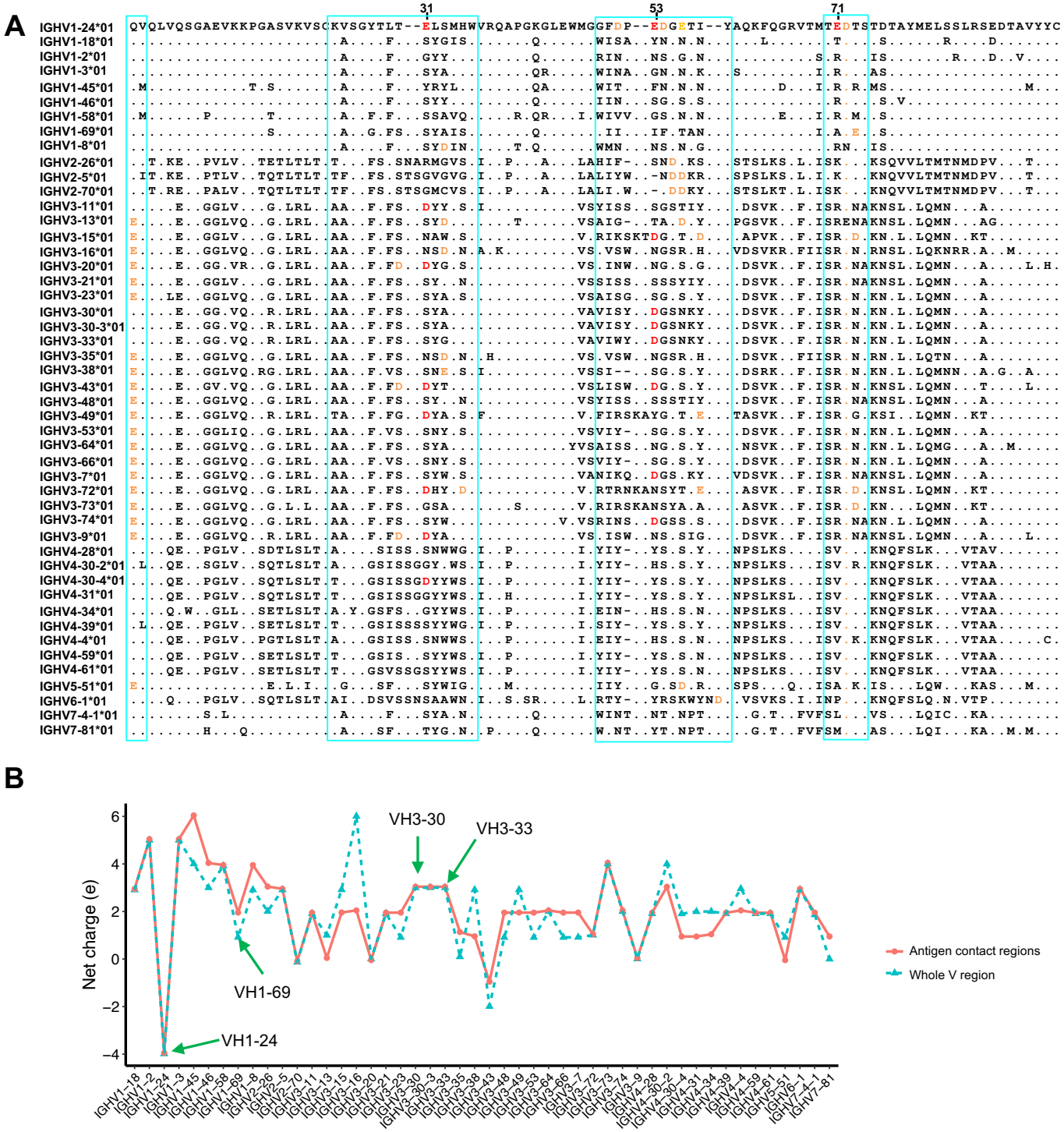

Figure S5. VH1-24 is the most negatively charged germline gene, Related to Figure 1.

(A) Multiple sequence alignment of the *01 allele for all VH genes. The cyan boxes show antigen contact regions defined by Sela-Culang et al. (2013), which include additional interactions not accounted for in the CDRs. The dots represent conserved residues compared with the VH1-24 gene. The negative charge residues at Kabat position 31, 53 and 71 are colored in red, and other negative charge residues within antigen contact regions are colored in orange.

(B) Net charge distribution of all VH genes. The cyan triangles represent the net charge of the whole V region, the red dots represent the net charge in antigen contact regions in panel A. The green arrows highlight the VH1-24, VH1-69, VH3-30 and VH3-33 germline genes.

A

Antibody	ka ($M^{-1}s^{-1}$)	kd (s^{-1})	K_D^{app} (nM)
1-87	114444	6.1775E-06	0.1359
1-87 IH30T	80919	6.1775E-06	0.0763
1-87 AH55G	65323	1.2732E-04	1.9490
1-87 IH30T AH55G	52927	1.1720E-04	2.2145
1-68	99785	2.4129E-04	2.4181
1-68 IH30T	71112	7.4050E-04	10.4131
1-68 AH55G	75649	4.2248E-04	5.5848
1-68 IH30T AH55G	78662	3.1756E-03	40.3702
2-51	149981	5.4046E-04	3.6035
2-51 IH30T	20299	2.9341E-03	14.4540
2-51 VH55G	230715	3.7759E-03	16.3660
2-51 IH30T VH55G	367225	2.6717E-02	72.7536
4-18	34869	1.4859E-07	0.0043
4-18 HH58Y AL29P TL91A NL93S	42767	1.7901E-03	41.8578
5-24	106110	4.4160E-05	0.4162
5-24 LH27F KH56N	97333	4.2056E-04	4.3208
2-17	36080	1.1175E-08	0.0003
2-17 NH51I DL32N	106299	7.5238E-04	7.0779
4-8	125519	5.6236E-04	4.4802
4-8 HH32Y TH35S NL52S	127990	2.6868E-03	20.9922
4A8	355683	5.0827E-04	1.4290

B

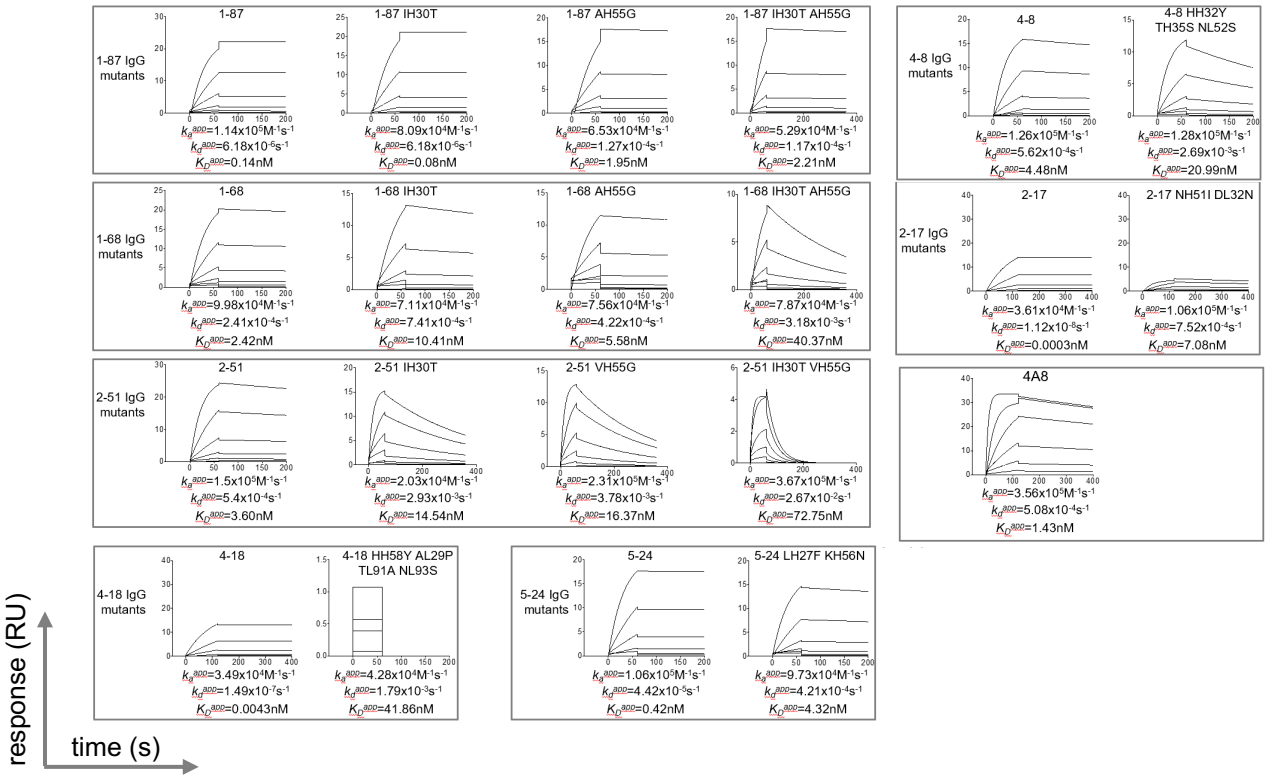

C

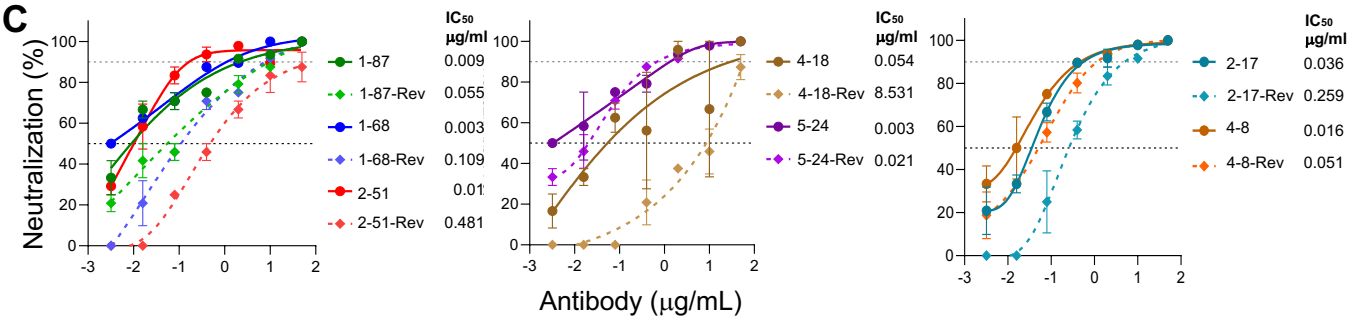

Figure S6. Effects of somatic hypermutation on binding affinity and neutralization potency of NTD antibodies, Related to Figures 1, 2, 3 and 6.

(A) Apparent SARS-CoV-2 spike binding affinity of NTD-directed antibodies (IgGs) show that somatic hypermutations significantly improve binding affinity.

(B) Surface plasmon resonance profiles of NTD-directed antibodies and revertants.

(C) Authentic virus neutralization profiles of NTD-directed antibodies show that somatic hypermutations significantly improve neutralization potency. Wildtype antibodies are solid line and germline reverted antibodies are dotted line. Mean±SEM is shown for each data point.

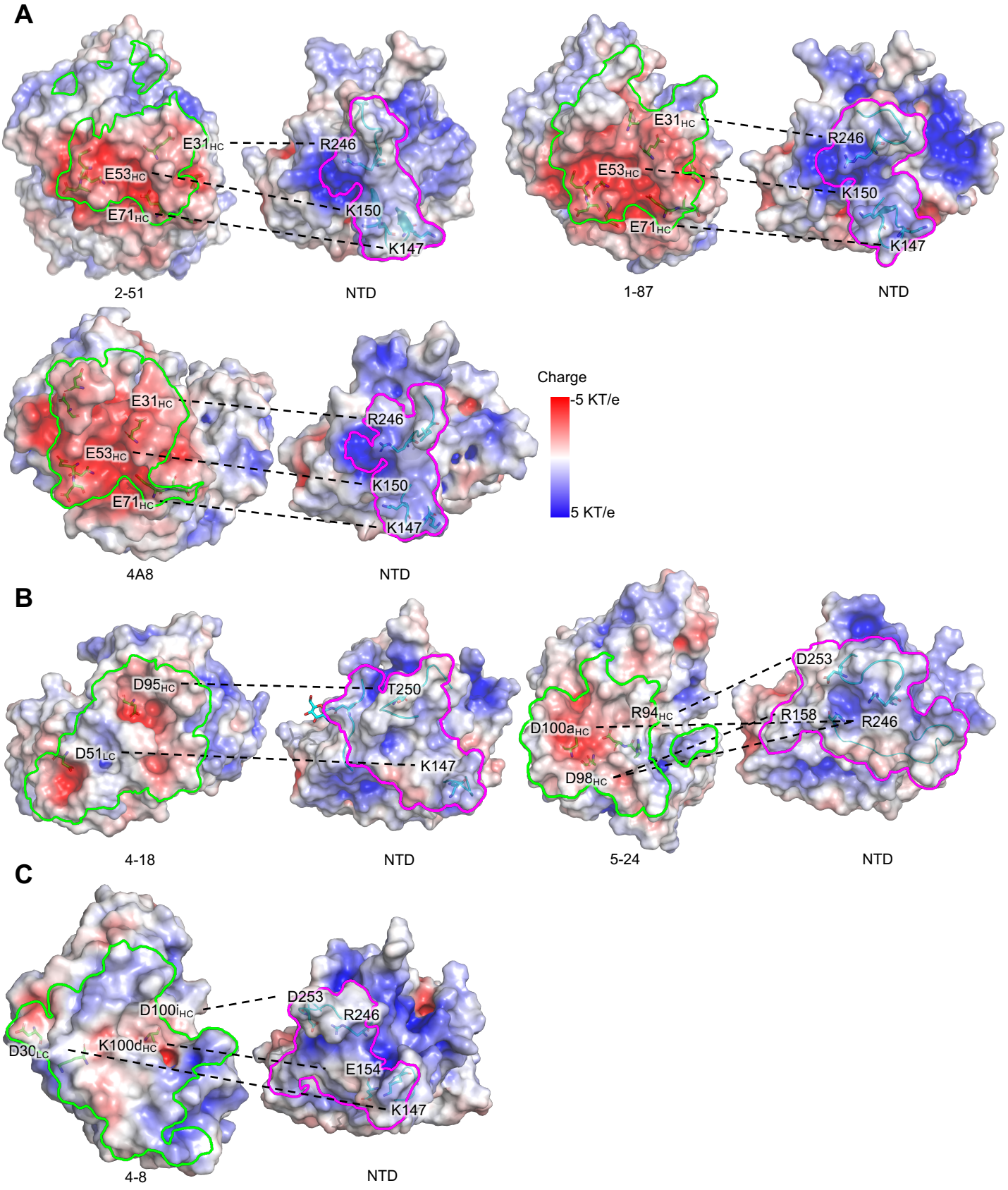

Figure S7. NTD-directed neutralizing antibodies are electronegative and target the electropositive supersite, Related to Figures 1, 2, 3 and 6.

(A) Electrostatic potential for VH1-24-derived antibodies. The blue surface shows electropositive charge potential, and the red shows negative charge potential. The paratope and epitope are highlighted by green and magenta boundaries, respectively. Residues involved in charge-charge interactions between antibody and NTD are linked by dashed lines.

(B) Electrostatic potential for VH3-30 (4-18) and VH3-33 (5-24) derived antibodies.

(C) Electrostatic potential for VH1-69-derived antibodies.

Table S1. Cryo-EM Data Collection and Refinement Statistics, Related to Figures 1-3.

SARS-CoV-2 S2P complex	1-87 Fab	4-18 Fab	5-24 Fab	4-8 Fab	2-17 Fab	1-68 Fab	2-51 Fab
EMDB ID	EMD-23125	EMD-23126	EMD-23127	EMD-23489	EMD-23490	EMD-23150	EMD-23151
PDB ID	7L2D	7L2E	7L2F	7LQV	7LQW		
Data Collection							
Microscope	FEI Titan Krios	FEI Titan Krios	FEI Titan Krios	FEI Titan Krios	FEI Titan Krios	FEI Titan Krios	FEI Titan Krios
Voltage (kV)	300	300	300	300	300	300	300
Electron dose ($e^-/Å^2$)	41.92	41.92	41.92	52.56	51.69	41.92	41.92
Detector	Gatan K3 BioQuantum	Gatan K3 BioQuantum	Gatan K3 BioQuantum	Gatan K3 BioQuantum	Gatan K3 BioQuantum	Gatan K3 BioQuantum	Gatan K3 BioQuantum
Pixel Size (Å)	1.07	1.07	1.07	1.058	1.058	1.07	1.07
Defocus Range (μm)	-0.8/-2.5	-0.8/-2.5	-0.8/-2.5	-0.1/-3.6	-0.3/-3.9	-0.8/-2.5	-0.8/-2.5
Magnification	81000	81000	81000	81000	81000	81000	81000
Reconstruction							
Software	cryoSPARC v2.15	cryoSPARC v2.15	cryoSPARC v2.15	cryoSPARC v2.15	cryoSPARC v2.15	cryoSPARC v2.15	cryoSPARC v2.15
Particles	62,479	280,327	115,545	88,375	29,767	34,450	190,557
Symmetry	C1	C3	C1	C1	C1	C1	C1*
Box size (pix)	390	392	400	380	400	440	384
Resolution (Å) ($FSC_{0.143}$)	3.63	2.97	3.93	3.25	4.47	3.80	3.71
Refinement							
Software	Phenix 1.18	Phenix 1.18	Phenix 1.18	Phenix 1.18	Phenix 1.18		
Protein residues	3492	4050	3970	3981	3409		
Chimera CC	0.85	0.80	0.86	0.81	0.74		
EMRinger Score	2.43	3.18	1.17	2.07	0.91		
R.m.s. deviations							
Bond lengths (Å)	0.006	0.007	0.008	0.004	0.003		
Bond angles (°)	1.16	1.29	1.27	0.7	0.81		
Validation							
Molprobity score	1.41	1.36	1.41	1.75	1.67		
Clash score	4.64	4.30	4.47	6.1	5.89		
Favored rotamers (%)	100	100	100	100	99		
Ramachandran							
Favored regions (%)	97.0	97.2	96.9	94.44	94.93		
Allowed regions (%)	3.0	2.8	3.1	5.53	5.04		
Disallowed regions (%)	0	0	0	0.03	0.03		

* The overall map is C1-symmetric but symmetry expansion in C3 was applied to the particles before local classification and local refinement to maximize the number of NTD-bound Fabs .

Table S2. X-ray Diffraction Data Collection and Refinement Statistics, Related to Figure 1.

	SARS-CoV-2 NTD in complex with 2-51 Fab
PDB ID	7L2C
Data Collection	
Space group	$P2_1$
Unit cell dimensions	
a,b,c (Å)	66.8, 115.8, 137.6
α,β,γ (°)	90, 100.0, 90
Resolution range (Å)	88.03-3.44 (3.57-3.44)*
Total reflections	49329 (2732)
Unique reflections	25964 (1550)
Completeness (%)	93.3 (47.4)
Redundancy	1.9 (1.8)
$I/\sigma(I)$	2.6 (0.8)
R_{merge}	0.233 (1.00)
R_{pim}	0.184 (0.529)
$CC_{1/2}$	0.883 (0.322)
Wilson B-factor (Å^2)	69
Refinement	
Resolution range (Å)	88.03-3.65
Number of complexes per asymmetric unit	2
R_{work}/R_{free}	21.6/27.2
Number of atoms	
Protein	11041
Ligands	300
Water	41
B-factors (Å^2)	
Protein	69
Ligands	94
Water	49
R.m.s. deviations	
Bond lengths (Å)	0.009
Bond angles (°)	1.48
Ramachandran statistics	
Favored (%)	94.11
Allowed (%)	5.89
Outliers (%)	0

* Values in parentheses are for the highest-resolution shell.

Table S3. Epitope residues* for eight potent NTD-directed neutralizing antibodies, Related to Figure 6.

1-87		1-68		2-51		2-17	
143	VAL	143	VAL	144	TYR	14	GLN
144	TYR	144	TYR	145	TYR	15	CYS
145	TYR	145	TYR	146	HIS	16	VAL
146	HIS	146	HIS	147	LYS	17	ASN
147	LYS	147	LYS	148	ASN	18	LEU
148	ASN	148	ASN	150	LYS	19	THR
149	ASN	150	LYS	152	TRP	20	THR
150	LYS	152	TRP	246	ARG	67	ALA
152	TRP	245	HIS	247	SER	74	ASN
158	ARG	246	ARG	248	TYR	75	GLY
245	HIS	248	TYR	249	LEU	76	THR
246	ARG	249	LEU	250	THR	77	LYS
248	TYR	250	THR	251	PRO	78	ARG
249	LEU	251	PRO	252	GLY	79	PHE
250	THR	252	GLY	253	ASP	140	PHE
251	PRO	253	ASP			144	TYR
252	GLY	254	SER			152	TRP
253	ASP	255	SER			154	GLU
254	SER	256	SER			156	GLU
255	SER					158	ARG
256	SER					244	LEU
258	TRP					246	ARG
						247	SER
						249	LEU

4A8		4-18		4-8		5-24	
143	VAL	14	GLN	12	GLN	14	GLN
144	TYR	15	CYS	13	CYS	15	CYS
145	TYR	16	VAL	144	TYR	16	VAL
146	HIS	17	ASN	145	TYR	17	ASN
147	LYS	18	LEU	146	HIS	144	TYR
148	ASN	19	THR	147	LYS	145	TYR
150	LYS	140	PHE	148	ASN	146	HIS
151	SER	142	GLY	152	TRP	147	LYS
152	TRP	143	VAL	154	GLU	148	ASN
158	ARG	144	TYR	155	SER	150	LYS
245	HIS	145	TYR	156	GLU	152	TRP
246	ARG	146	HIS	157	PHE	154	GLU
247	SER	147	LYS	158	ARG	155	SER
248	TYR	148	ASN	160	TYR	156	GLU
249	LEU	150	LYS	161	SER	158	ARG
250	THR	154	GLU	162	SER	161	SER
251	PRO	156	GLU	246	ARG	162	SER
256	SER	158	ARG	247	SER	246	ARG
257	GLY	244	LEU	248	TYR	248	TYR
		245	HIS	249	LEU	249	LEU
		246	ARG	250	THR	250	THR
		247	SER	251	PRO	251	PRO
		248	TYR	252	GLY	252	GLY
		249	LEU	253	ASP	253	ASP
		250	THR	254	SER	254	SER
		251	PRO			256	SER
		252	GLY				
		253	ASP				
		256	SER				

*Epitope residues were defined by buried surface accessibility (PISA). For antibodies 1-68 and 2-17 the resolution was too low to allow EM density-based modeling. Therefore, structural models for such antibodies were produced either by homology modeling (for 1-68) or poly-Ala modeling followed by template-based model generation (for 2-17). Within these eight complexes, the number of epitope residues ranged from 15 (for antibody 2-51) to 29 (for antibody 4-18), with an average of 22.4.

Table S4. Pairwise intersection of epitope residues* for eight potent NTD-directed neutralizing antibodies, Related to Figures 6 and 7.

(4A8, 4-18)	
143	VAL
144	TYR
145	TYR
146	HIS
147	LYS
148	ASN
150	LYS
158	ARG
245	HIS
246	ARG
247	SER
248	TYR
249	LEU
250	THR
251	PRO
256	SER

(4A8, 4-8)	
144	TYR
145	TYR
146	HIS
147	LYS
148	ASN
152	TRP
158	ARG
246	ARG
247	SER
248	TYR
249	LEU
250	THR
251	PRO

(4A8, 5-24)	
144	TYR
145	TYR
146	HIS
147	LYS
148	ASN
150	LYS
152	TRP
158	ARG
246	ARG
248	TYR
249	LEU
250	THR
251	PRO
256	SER

(4A8, 1-87)	
143	VAL
144	TYR
145	TYR
146	HIS
147	LYS
148	ASN
150	LYS
152	TRP
158	ARG
245	HIS
246	ARG
248	TYR
249	LEU
251	PRO
256	SER

(4A8, 1-68)	
143	VAL
144	TYR
145	TYR
146	HIS
147	LYS
148	ASN
150	LYS
152	TRP
245	HIS
246	ARG
248	TYR
249	LEU
250	THR
251	PRO
256	SER

(4A8, 2-51)	
144	TYR
145	TYR
146	HIS
147	LYS
148	ASN
150	LYS
152	TRP
246	ARG
247	SER
248	TYR
249	LEU
250	THR
251	PRO

(4A8, 2-17)	
144	TYR
152	TRP
158	ARG
246	ARG
247	SER
249	LEU

(4-18, 4-8)	
144	TYR
145	TYR
146	HIS
147	LYS
148	ASN
154	GLU
156	GLU
158	ARG
246	ARG
247	SER
248	TYR
249	LEU
250	THR
251	PRO
252	GLY
53	ASP

(4-18, 5-24)	
14	GLN
15	CYS
16	VAL
17	ASN
144	TYR
145	TYR
146	HIS
147	LYS
148	ASN
150	LYS
154	GLU
156	GLU
158	ARG
246	ARG
248	TYR
249	LEU
250	THR
251	PRO
252	GLY
253	ASP
256	SER

(4-18, 1-87)	
143	VAL
144	TYR
145	TYR
146	HIS
147	LYS
148	ASN
150	LYS
158	ARG
245	HIS
246	ARG
248	TYR
249	LEU
250	THR
251	PRO
252	GLY
253	ASP
256	SER

(4-18, 1-68)	
143	VAL
144	TYR
145	TYR
146	HIS
147	LYS
148	ASN
150	LYS
245	HIS
246	ARG
248	TYR
249	LEU
250	THR
251	PRO
252	GLY
253	ASP
256	SER

(4-18, 2-51)	
144	TYR
145	TYR
146	HIS
147	LYS
148	ASN
150	LYS
246	ARG
247	SER
248	TYR
249	LEU
250	THR
251	PRO
252	GLY
253	ASP

(4-18, 2-17)	
14	GLN
15	CYS
16	VAL
17	ASN
18	LEU
19	THR
140	PHE
144	TYR
154	GLU
156	GLU
158	ARG
244	LEU
246	ARG
247	SER
249	LEU

(2-51, 2-17)	
144	TYR
152	TRP
246	ARG
247	SER
249	LEU

(4-8, 5-24)	
144	TYR
145	TYR
146	HIS
147	LYS
148	ASN
152	TRP
154	GLU
155	SER
156	GLU
158	ARG
161	SER
162	SER
246	ARG
248	TYR
249	LEU
250	THR
251	PRO
252	GLY
253	ASP
254	SER

(4-8, 1-87)	
144	TYR
145	TYR
146	HIS
147	LYS
148	ASN
152	TRP
158	ARG
246	ARG
248	TYR
249	LEU
250	THR
251	PRO
252	GLY
253	ASP
254	SER

(4-8, 1-68)	
144	TYR
145	TYR
146	HIS
147	LYS
148	ASN
152	TRP
246	ARG
248	TYR
249	LEU
250	THR
251	PRO
252	GLY
253	ASP
254	SER

(4-8, 2-51)	
144	TYR
145	TYR
146	HIS
147	LYS
148	ASN
152	TRP
246	ARG
247	SER
248	TYR
249	LEU
250	THR
251	PRO
252	GLY
253	ASP

(4-8, 2-17)	
144	TYR
152	TRP
154	GLU
156	GLU
158	ARG
246	ARG
247	SER
249	LEU

(1-68, 2-51)	
144	TYR
145	TYR
146	HIS
147	LYS
148	ASN
150	LYS
152	TRP
246	ARG
248	TYR
249	LEU
250	THR
251	PRO
252	GLY
253	ASP

(1-68, 2-17)	
144	TYR
152	TRP
246	ARG
249	LEU

(5-24, 1-87)	
144	TYR
145	TYR
146	HIS
147	LYS
148	ASN
150	LYS
152	TRP
158	ARG
246	ARG
248	TYR
249	LEU
250	THR
251	PRO
252	GLY
253	ASP
254	SER
256	SER

(5-24, 1-68)	
144	TYR
145	TYR
146	HIS
147	LYS
148	ASN
150	LYS
152	TRP
246	ARG
248	TYR
249	LEU
250	THR
251	PRO
252	GLY
253	ASP
254	SER
256	SER

(5-24, 2-51)	
144	TYR
145	TYR
146	HIS
147	LYS
148	ASN
150	LYS
152	TRP
246	ARG
248	TYR
249	LEU
250	THR
251	PRO
252	GLY
253	ASP

(5-24, 2-17)	
14	GLN
15	CYS
16	VAL
17	ASN
144	TYR
152	TRP
154	GLU
156	GLU
158	ARG
246	ARG
249	LEU

(1-87, 1-68)	
143	VAL
144	TYR
145	TYR
146	HIS
147	LYS
148	ASN
150	LYS
152	TRP
245	HIS
246	ARG
248	TYR
249	LEU
250	THR
251	PRO
252	GLY
253	ASP
254	SER
255	SER
256	SER

(1-87, 2-51)	
144	TYR
145	TYR
146	HIS
147	LYS
148	ASN
150	LYS
152	TRP
246	ARG
248	TYR
249	LEU
250	THR
251	PRO
252	GLY
253	ASP

(1-87,2-17)	
144	TYR
152	TRP
158	ARG
246	ARG
249	LEU

*For antibodies 1-68 and 2-17 the resolution was too low to allow EM density-based modelling. Therefore, structural models for such antibodies were produced either by homology modeling (for 1-68) or poly-Ala modeling followed by template-based model generation (for 2-17).

Table S5. NTD supersite defined by either the intersection of eight NTD-directed antibodies or by the union of pairwise intersections, Related to Figures 6 and 7.

The term “supersite” has been widely used in the influenza virus and HIV antibody fields to denote common share epitopes (Kong et al., 2013; Kumar et al., 2020; Lee et al., 2015; Longo et al., 2016; Moyo et al., 2020; Zhou et al., 2014; Zhou et al., 2016). Here we assess two definitions of the “NTD-supersites”, one defined by the intersection of the eight NTD-directed antibodies and the other defined by the union of the pairwise intersection of epitopes.

NTD-supersite defined by the intersection of all 8 antibodies	
144	TYR
246	ARG
249	LEU

The intersection defined only 3 residues, much lower than the average number of residues in these NTD-epitopes (22.4 residues) (Table S3). Interestingly, 2 of these 3 residues are the exact residues mutated in emerging variants of concern (del144 and R246I), and L249 is likely affected by del242-244.

By contrast, the union of pairwise interactions defined 34 residues; this was about 50% larger than a typical epitope, but nevertheless seemed to capture the overall character of the NTD supersite.

NTD-supersite defined by the union of the pairwise intersection of all 8 antibodies	
14	GLN
15	CYS
16	VAL
17	ASN
18	LEU
19	THR
140	PHE
143	VAL
144	TYR
145	TYR
146	HIS
147	LYS
148	ASN
150	LYS
152	TRP
154	GLU
155	SER
156	GLU
158	ARG
161	SER
162	SER
244	LEU
245	HIS
246	ARG
247	SER
248	TYR
249	LEU
250	THR
251	PRO
252	GLY
253	ASP
254	SER
255	SER
256	SER

Table S6. Kinetic parameters and affinities for the binding of NTD-directed antibody Fabs to SARS-CoV-2 spike, Related to Figures 6 and 7.

Fab	k_a ($M^{-1}s^{-1}$)	k_d (s^{-1})	K_D (nM)
1-87	$5.76(4)\times10^{4}$	$1.40(6)\times10^{-4}$	2.44(2)
1-68	$5.69(2)\times10^{4}$	$7.86(2)\times10^{-4}$	13.83(3)
2-51	$9.11(2)\times10^{4}$	$2.67(2)\times10^{-3}$	29.32(3)
4-18	$1.71(1)\times10^{4}$	$1.07(4)\times10^{-4}$	6.26(3)
5-24	$5.83(4)\times10^{4}$	$6.71(6)\times10^{-5}$	1.15(1)
2-17	$4.0(1)\times10^{3}$	$1.25(3)\times10^{-3}$	317(4)
4-8	$3.51(3)\times10^{4}$	$2.99(2)\times10^{-3}$	85.0(3)
4A8	$7.88(3)\times10^{4}$	$2.82(4)\times10^{-3}$	35.83(5)